PERFORMANCE ANALYSIS OF A REPEAT-PASS INSAR MISSION FOR DEFORMATION AND TOPOGRAPHY MAPPING OF SATURN'S MOON ENCELADUS

Andreas Benedikter°, Paul Rosen⋆, Mark Simons†, Ryan Park⋆, Marc Rodriguez-Cassola°, Pau Prats-Iraola°, Gerhard Krieger°, Jalal Matar°

°Microwaves and Radar Institute, German Aerospace Center (DLR)
⋆Jet Propulsion Laboratory, California Institute of Technology
†Seismological Laboratory, California Institute of Technology

ABSTRACT

Over the last decades, repeat-pass SAR interferometry (InSAR) for deformation measurement and topographic mapping has revolutionized our understanding of many geophysical processes on Earth. A new mission concept, currently in development at the Jet Propulsion Laboratory (JPL) and Caltech, aims at using orbital repeat-pass InSAR for deformation and topography mapping of Saturn's ice-covered and geologically active moon Enceladus. In this paper, we present an initial performance assessment of the system and the suggested SAR processing approach, along with simulated InSAR acquisitions using a DLR in-house End-to-End performance simulator.

***Index Terms*—** SAR, SAR interferometry, Saturn, Enceladus, Planetary Mission

1. INTRODUCTION

With a diameter of only about $500\,\mathrm{km}$, Saturn's moon Enceladus is a differentiated geologically active body, most likely comprising a porous rocky core and an ice shell, separated by a global subsurface water ocean [1] (cf. Fig. 1). The discovery of plumes ejecting gas and ice particles through cracks within the ice crust in the south polar region and the presence of complex organic molecules within [2] have assigned a high priority to Enceladus among exploratory mission plans investigating habitability of other worlds. A new mission concept, currently in development at the Jet Propulsion Laboratory (JPL) and Caltech, aims at using –among other modalities– repeat-pass SAR interferometry (InSAR) for deformation and topography mapping to understand the state of habitability of Enceladus, and to expand our knowledge on its past and present structural, dynamical, and kinematical properties.

Enceladus presents several distinctive observational characteristics that favor the use of repeat-pass InSAR. These include an almost-absent atmosphere, negligible temporal decorrelation effects in most areas, high backscatter (above $0\,\mathrm{dB}$ were measured in Ku- and S-band [3, 4]), and short orbital repeat cycles of approximately 30 hours. However,

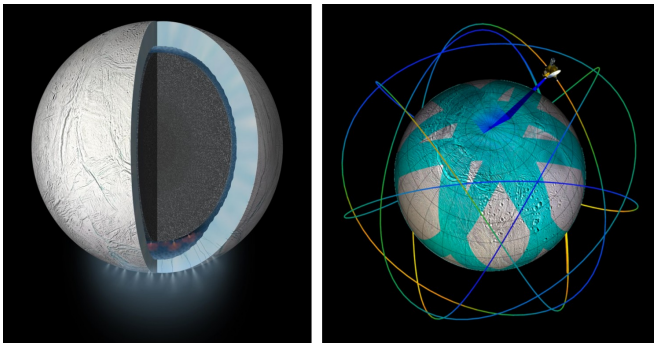

Fig. 1: (Left) artist's conception of Enceladus and its inner structure (image credit: NASA JPL) and (right) illustration of the spacecraft in the candidate orbit around Enceladus.

several aspects of the environment may lead to increased system and mission complexity that must be studied carefully and accounted for in the system design. These include: i) strong third-body gravitational perturbation from Saturn, which limits the number of feasible orbits and high orbital inclinations (e.g., above $60°$ for repeat orbits). One candidate repeat orbit has been proposed in [5] and is shown in Fig. 1 and Fig. 2; ii) the large distance to Earth paired with the uncertainties in the gravitational models limit orbit controlability and orbit determination accuracy; iii) the limited down-link capacity from the Saturnian system to Earth requires tailored on-board processing strategies for both SAR focusing and InSAR processing to reduce the data rate.

The system and performance discussions in the following are focused on aspects that are particular to SAR and InSAR surveys over Enceladus.

2. SAR SYSTEM CONSIDERATIONS AND PERFORMANCE

The preliminary radar system specifications are depicted in Table 1. An S-band frequency is chosen as a compromise among phenomenological (i.e., volume decorrelation, backscattered power, etc.) and technological (i.e., interfer-

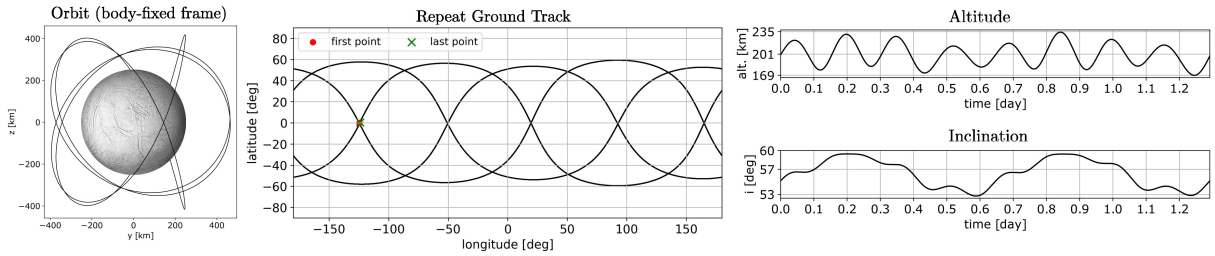

Fig. 2: One repeat cycle of the candidate orbit [5].

ometric baseline, baseline determination accuracy, on-board processing demands, etc.) constraints.

Table 1: Preliminary radar system parameters.

Parameter	Value	Comment
Wavelength	0.13 m	
Pulse repetition frequency	500 Hz	Oversampling for presumming
Range bandwidth	30 MHz	
Pulse duration	60 μs	
Tx peak power	200 W	
Receiver noise temperature	240 K	
Look angle	24.4 deg	
Equivalent antenna length	~3.5 m	Radar operated on high-gain telecom antenna (4-m reflector)
Equivalent antenna height	~0.5 m	Sub-illumination of reflector to achieve ~80 km swath width
Antenna efficiency	-3 dB	
Losses (feed, cable)	-1.5 dB	
System power margin	5 dB	

The 4-m high-gain reflector antenna will be shared for radar operations and telecommunication. In elevation direction, the reflector is partially illuminated to achieve a swath width of roughly $80\,\mathrm{km}$ in stripmap operation when pointed with a look angle of $24.4°$. The resulting coverage of the most-interesting south polar region is shown in Fig. 1. Note that this region can be potentially covered from five different passes of the orbiter. The different viewing geometries may be used to derive 3-D deformation vectors, mitigate shadow problems, and disentangle deformation and topography signatures. To reduce the data rate, both SAR and InSAR processing will be performed on board up to multi-looked interferograms.

2.1. SAR Performance Aspects

The resulting noise equivalent sigma naught (NESN) across the swath is shown in Fig. 3 (left) for the minimum, mean, and maximum orbit altitudes. The pointing of the antenna and the swath are optimized for the $200\,\mathrm{km}$ altitude to achieve the

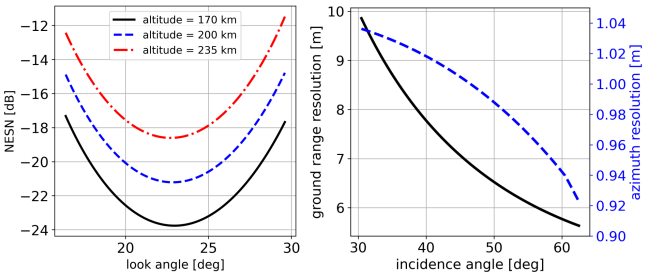

Fig. 3: SAR system performance across the swath derived from the parameters in Table 1 and for a near south polar pass of the orbit in Fig. 2: (left) the NESN for different orbit altitudes and (right) the ground resolution in range and azimuth.

$80\,\mathrm{km}$ swath width and to cover the pole. For achieving an azimuth ambiguity to signal ratio (AASR) of $-25\,\mathrm{dB}$, a pulse repetition frequency (PRF) of roughly $90\,\mathrm{Hz}$ is required. Note that the orbiter velocity is only around $120\,\mathrm{m\,s^{-1}}$. As a consequence of the small size of Enceladus, range ambiguities do not contribute to the ambiguity budget up to a PRF of approximately $900\,\mathrm{Hz}$, since they would be placed beyond the limb of the body. Hence, a substantial oversampling in azimuth with a PRF of $500\,\mathrm{Hz}$ can be used to reduce the peak power.

Fig. 3 (right) shows the potential ground resolution in range and azimuth direction for a south polar pass of the orbiter and an altitude of $200\,\mathrm{km}$, where the swath in far range is reaching beyond the South Pole (spacecraft position as illustrated in Fig. 1). The achievable azimuth resolution is significantly better compared to the standard formulation of half of the antenna length due to an almost $50\,\%$ lower ground velocity compared to the orbital velocity, caused by the relatively small body size to orbit height ratio.

2.2. SAR Focusing Aspects

The proposed SAR focusing chain is based on the chirp scaling algorithm, including two additional steps in order to accommodate the non-negligible eccentricity of the orbit paired with the relatively long integration times of the SAR surveys, namely: i) a residual hyperbolic correction in the range-Doppler domain and ii) the subaperture topography- and aperture-dependent (SATA) algorithm [6].

SATA was developed in the frame of airborne SAR systems to compensate for non-ideal trajectory deviations during

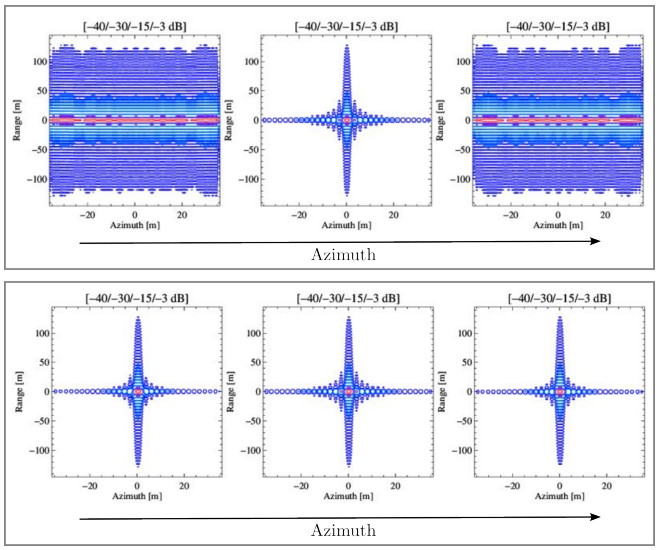

Fig. 4: Validation of the proposed SAR focusing approach using simulated point targets at mid-range of the swath, spread along a $20\,\mathrm{km}$ processing interval in azimuth, showing the effect of SATA [6] for compensating space-variant effects: (top) without using SATA and (bottom) when SATA is applied.

SAR focusing by considering the topography of the scene and the wide antenna beamwidth [6, 7]. SATA works with short-time Fourier transforms along azimuth before azimuth compression to compensate the non-ideal trajectory in both the space and Doppler domain. For the Enceladus SAR surveys, SATA is an efficient approach to accommodate space-variant effects within the synthetic aperture observation time resulting from the eccentricity of the orbit. Fig. 4 shows point target simulations based on the system in Table 1 and the orbit in Fig. 2. The top panel shows the results when the focusing is performed without SATA and the bottom panel when SATA is applied. The point targets are placed along the $20\,\mathrm{km}$ processing interval in azimuth at mid-range of the swath. Without using SATA, the point targets that are not located in the center of the azimuth interval experience strong defocusing, a direct consequence of the space-variance. Note that this effect cannot be compensated by processing smaller blocks in azimuth, since the azimuth variance occurs within the synthetic aperture observation time. With SATA, the space-variance can be efficiently compensated and the point targets appear well focused.

2.3. InSAR Performance Aspects

The orbit in Fig. 2 is periodic in an Enceladus body-fixed frame and can potentially provide repeat passes every 30 hours. However, the large distance to Earth paired with the uncertainties in the gravitational models do not allow for a very tight orbit control. The control accuracy of the baseline between repeating passes is expected to be roughly $130\,\mathrm{m}$ (1 sigma). In contrast to Earth observation applications, temporal decorrelation effects are expected to be negligible due to the absence of common decorrelation sources in glacial terrain (e.g., significant snow fall or melt events). The high backscatter values reported for the Enceladus surface (above $0\,\mathrm{dB}$) suggest that the backscatter is dominated by efficient volume scattering in the upper part of the Enceladus ice crust [3, 4] that will introduce decorrelation for baselines greater than zero, depending on the penetration depth into the scattering volume. In the following, we assume a uniformly scattering ice volume and a 2-way penetration depth (i.e., the depth after which the power is decreased by a factor of $\frac{1}{e}$) of $15\,\mathrm{m}$. This assumption is rather conservative when comparing to penetration values reported at S band in high backscatter glacial areas on Earth. However, to this date, the scattering mechanisms on Enceladus are poorly understood and mitigation strategies for potentially larger penetration need to be implemented. Fig. 5 shows the expected relative errors for the displacement and height measurement across the swath for a variety of baselines, a product resolution of $20\,\mathrm{m}$ x $20\,\mathrm{m}$, a backscatter of $0\,\mathrm{dB}$, and including common decorrelation sources except temporal decorrelation. Note that the volume decorrelation is dominating the budget. A displacement measurement error of less than few millimeters is to be expected and a topographic mapping capability with an accuracy of less than few meters. Note that the height estimated with InSAR will be systematically biased downward with respect to the surface due to the penetration into the volume and uncompensated propagation effects through the dielectric interface at the surface.

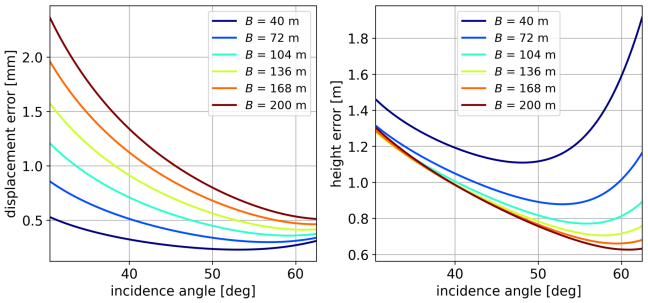

Fig. 5: InSAR performance across the swath for the system in Table 1 assuming a product resolution of $20\,\mathrm{m}$ x $20\,\mathrm{m}$ and an uniform scattering volume with exponential extinction properties with a penetration depth of $15\,\mathrm{m}$: (left) displacement measurement error and (right) height measurement error for different baselines, B.

3. END-TO-END SIMULATION OF REALISTIC INSAR ACQUISITIONS

We use an in-house End-to-End (E2E) simulator developed at the Microwaves and Radar Institute of DLR [8] to generate realistic SAR products from the raw data to stacks of InSAR acquisitions. The simulations are used to evaluate the

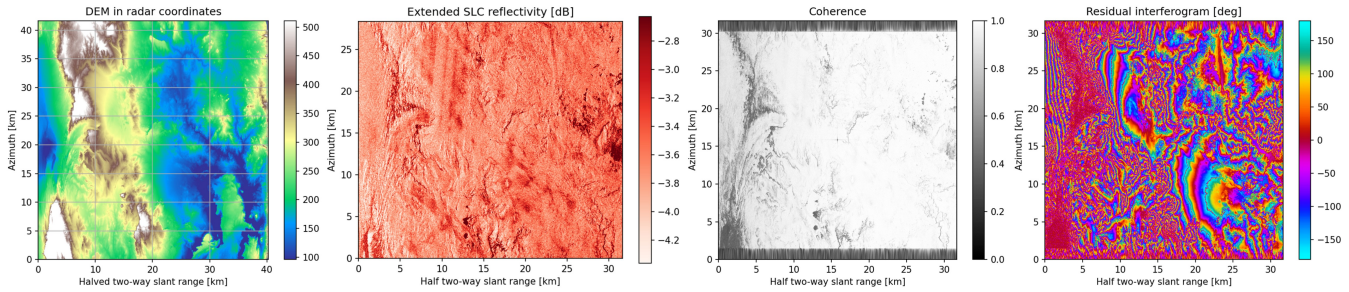

Fig. 6: First End-2-End simulation of a repeat-pass InSAR acquisition at Enceladus assuming the system in Table 1, the orbit in Fig. 2, an ellipsoidal model of Enceladus modulated with the DEM in the left panel, and a horizontal baseline of $200\,\mathrm{m}$.

system performance and derive suitable interferometric processing strategies. The E2E is capable of accommodating the orbital geometries, an arbitrary topography, realistic deformation models, representative backscatter maps, and decorrelation effects, as well as any relevant instrument, baseline, and attitude errors. Fig. 6 shows first simulation results using the E2E and assuming the system in Table 1, the orbit in Fig. 2, and an ellipsoidal model of Enceladus modulated with representative topography derived from a digital elevation model (DEM) of the *Shuttle Radar Topography Mission* (SRTM). The DEM (with respect to the ellipsoid) is shown in the left panel. The reflectivity is generated synthetically, based on the local topography. The two panels on the right show the resulting interferogram and coherence for a baseline of $200\,\mathrm{m}$ (mostly oriented horizontally) when using the ellipsoid for the SAR focusing and InSAR processing. Only a global offset estimation for coregistration is performed. The fringes in the interferogram can be attributed to the topography. In general, the interferogram looks clean, however, in areas with strong topography the fringe rates are high for the $200\,\mathrm{m}$ baseline, suggesting the use of low-resolution topographic maps (available from optical stereo imaging during the Cassini mission) for the on-board InSAR processing if also strong topography regions should be recovered consistently. Note that deformation and volume decorrelation effects have not been included yet in the simulation. The volume decorrelation will have impacts on the data quality, but is not expected to significantly impact the InSAR processing assumptions, as long as sufficient coherence for the offset estimation remains.

4. CONCLUSION

We have presented a first performance assessment of an interferometric SAR mission for deformation and topography mapping of Enceladus. The orbit and the geophysical properties of Enceladus introduce unique characteristics that need to be accounted for in the system design and accommodated in the processing strategies. The End-to-End simulation results show clean interferograms, thus providing an initial validation of the system and processing concept.

5. REFERENCES

[1] J. R. Spencer and F. Nimmo, "Enceladus: An active ice world in the Saturn system," *Annual Review of Earth and Planetary Sciences*, vol. 41, no. 1, pp. 693–717, 2013.

[2] F. Postberg et al., "Macromolecular organic compounds from the depths of Enceladus," *Nature*, vol. 558, pp. 564–568, 2018.

[3] K. L. Mitchell et al., "Enceladus' brilliant surface: Cassini RADAR observations and interpretation," in *44th Lunar and Planetary Science Conference*, Houston, 2013, p. Abstract #2902, Lunar and Planetary Institute.

[4] G. J. Black, D. B. Campbell, and L. M. Carter, "Arecibo radar observations of Rhea, Dione, Tethys, and Enceladus," *Icarus*, vol. 191, no. 2, pp. 702–711, 2007.

[5] A. Benedikter et al., "Periodic orbits for interferometric and tomographic radar imaging of Saturn's moon Enceladus," *Acta Astronautica*, vol. 191, pp. 326–345, 2022.

[6] P. Prats, A. Reigber, and J.J. Mallorqui, "Topography-dependent motion compensation for repeat-pass interferometric SAR systems," *IEEE Geoscience and Remote Sensing Letters*, vol. 2, no. 2, pp. 206–210, 2005.

[7] P. Prats et al., "Comparison of topography- and aperture-dependent motion compensation algorithms for airborne SAR," *IEEE Geoscience and Remote Sensing Letters*, vol. 4, no. 3, pp. 349–353, 2007.

[8] M. Rodriguez-Cassola et al., "End-to-end level-0 data simulation tool for future spaceborne SAR missions," in *EUSAR 2018; 12th European Conference on Synthetic Aperture Radar*, 2018, pp. 1–6.